Proceedings of
10th European Conference on Turbomachinery Fluid dynamics & Thermodynamics
ETC10, April 15-19, 2013, Lappeenranta, Finland

INFLUENCE OF THE CLEARANCE SIZE ON ROTATING INSTABILITY IN AN AXIAL COMPRESSOR STATOR

Ch. Beselt[*] - B. Pardowitz[⋆] - R. van Rennings[*] - R. Sorge[*]
D. Peitsch[*] - L. Enghardt[⋆] - F. Thiele[*] - K. Ehrenfried[,⋆] - P.-U. Thamsen[*]*

[*]Berlin Institute of Technology, Berlin, Germany
Email: christian.beselt@ilr.tu-berlin.de

[⋆]German Aerospace Center (DLR), Berlin, Germany

ABSTRACT

In order to improve the understanding of unsteady secondary flow structures in axial turbomachines, the flow in a scaled axial compressor stator was studied. It was operated in the vicinity of the stability line and could be equipped with variable hub clearances. Results from unsteady aerodynamic and acoustic pressure measurements, high-speed Particle Image Velocimetry measurements, and turbulence resolving numerical simulations are presented. Typical characteristics of the rotating instability (RI) phenomenon were found. A parameter study varying the clearance size and the blade loading, respectively, revealed the surprising occurrence of the RI even for the stator configuration without hub clearance. This contradicts the hitherto presumption of a hub or tip clearance needed to be in place for a rotating instability to emerge.

NOMENCLATURE

Symbols

a	Pa	azimuthal mode magnitude
A	Pa	magnitude
c_{xy}	m/s	in-plane velocity magnitude
Δf	Hz	frequency difference
G	1	mode transfer functions
i_M	°	incidence at midspan
l_c	m	chord length
m	1	azimuthal mode order
Ma	1	Mach number
p	Pa	static pressure
Re	1	Reynolds number
t	m	blade pitch
x, y, z	m	coordinate system
β	°	circumferential flow angle
γ^2	1	spectral coherence
γ_C	°	compressor blades stagger angle
τ	m	clearance size

Abbreviations

CSC	compressor cascade
HS-PIV	high-speed particle image velocimetry
LE	leading edge
PSD	power spectral density function
RI	rotating instability
SNR	signal to noise ratio
T	throttle
VIGV	variable inlet guide vanes

INTRODUCTION

A detailed understanding of the physics of rotating instability (RI) is a prerequisite for the development of more efficient, quieter and safer compressors. The RI phenomenon occurs at off-design conditions in compressors, predominantly in configurations with large tip or hub clearances. RI is regarded as a potential indicator for critical operating conditions like rotating stall and surge, since it occurs prior to such unstable operating conditions and does not affect the global stability of the compressor system. More precisely, at specific operating conditions non-synchronous blade vibrations are excited by the RI process, accompanied with increased broad-band noise levels. Generally, the

RI is characterized by unsteady pressure fluctuations in a rotating frame of reference relative to the rotor and casing. This fact distinguishes the RI from rotating stall, which exhibit a steady pressure field within the rotating stall cells, that extends in axial direction at least through the stalled blade row. According to Cumpsty (2004), the characteristic frequencies of rotating stall are about 30 to $150\,\mathrm{Hz}$, which is lower than the frequencies typically found for the RI. Although both phenomena, rotating instability as well as rotating stall, are capable of exciting large amplitude pressure fluctuations on the blading, they do not cause the instability of the overall compressor system. The latter is known as surge and features the fluctuating mass-flow even with negative mass-flow rates within the entire compressor system and is clearly different to rotating instability. Furthermore, in the literature the RI is detected by frequency spectra of single point measurements taken in the vicinity of the leading edge (LE), that exhibit characteristic signatures with side-by-side peaks. Each of which can be assigned to an circumferential mode. So far, there is no analytical model of the RI to predict the observed frequencies and modal structures, although van Rennings et al. (2012a) successfully made an approach to model the presumed RI mechanism numerically. According to existing explanations for the RI phenomenon, unsteady vortex structures in the clearance region are the basic source mechanism of the RI. Mailach et al. (2001) and März et al. (2002) reported a characteristic periodic vortex path in the passage coupled to the dominant frequencies in the spectral RI signature. Schrapp (2008) related the dominant RI frequencies to the clearance vortex breakdown in the blade passage. Results of Kameier (1994) on a shrouded rotor without a tip clearance vortex, however, question these existing explanations of the initiating mechanism of the RI. Kameier showed the occurrence of RI for high loadings of the rotor blades, although the fan did not operate in rotating stall conditions. Further investigations by Baumgartner et al. (1995) and Hofmann et al. (1998) found the inception of RI in the first stages of multi-stage high pressure compressors in stable operating conditions, which were clearly distinguished from rotating stall. However, similar spectral signatures were observed for compressors in the so-called mild stall condition. In that case, rotating disturbances appear and disappear intermittently between the stall inception point and the maximum pressure point, denoted as "short length scale disturbances" (SLSD) (Inoue et al. (2004)). Weidenfeller and Lawerenz (2002) detected the RI in an isolated stator configuration with hub clearance, using single unsteady pressure sensors in the blade passages.

The current investigation was pursued on an annular cascade with a variable hub clearance. In this setup, both the flow field next to the LE as well as the associated rotating pressure waves are captured. The identification and description of the main characteristics of the RI are given by Beselt and Peitsch (2012) and Pardowitz et al. (2012b). The objective of this paper is to give further insight into the RI phenomenon and its dependence on the gap width. Hub clearances of $3\,\%$ and $1\,\%$ blade height are investigated and compared to a configuration without clearance. Surprisingly, the characteristic spectral signatures of RI are detected in all these configurations. In a joint project of TU Berlin and DLR, these configurations are investigated using experimental and numerical methods. The setup without rotating parts promotes the integration of various measurement techniques to analyze both the steady and unsteady aerodynamic as well as acoustic properties coupled with the RI. With high-speed PIV (HS-PIV) equipment and unsteady pressure sensors the unsteady flow field in the blade passages are measured as well as associated rotating pressure waves. Validated numerical simulations enable a detailed insight into the unsteady flow fields at the stator blades.

EXPERIMENTAL SETUP AND PROCEEDURES

An experimental and numerical investigation was carried out on the annular compressor stator cascade of the Department of Aeronautics and Astronautics at the Berlin Institute of Technology. This test rig has been used in other publications investigating the RI, such as Beselt et al. (2011); Beselt and Peitsch (2012), Beselt et al. (2012), Sorge and Thamsen (2012), van Rennings et al. (2012b) and

Pardowitz et al. (2012a,b).

Test rig and Test conditions

The test rig depicted in Figure 1 (left) consists of three separate blade rows: Variable Inlet Guide Vanes (VIGV), the compressor stator cascade and a throttle. The incidence of the inflow impinging on the compressor blades is adjusted by changing the stagger angle of the VIGV, whereas the throttle is used to adjust the aerodynamic parameters within the test rig.
The compressor stator cascade consists of 20 prismatically shaped blades which are depicted in Figure

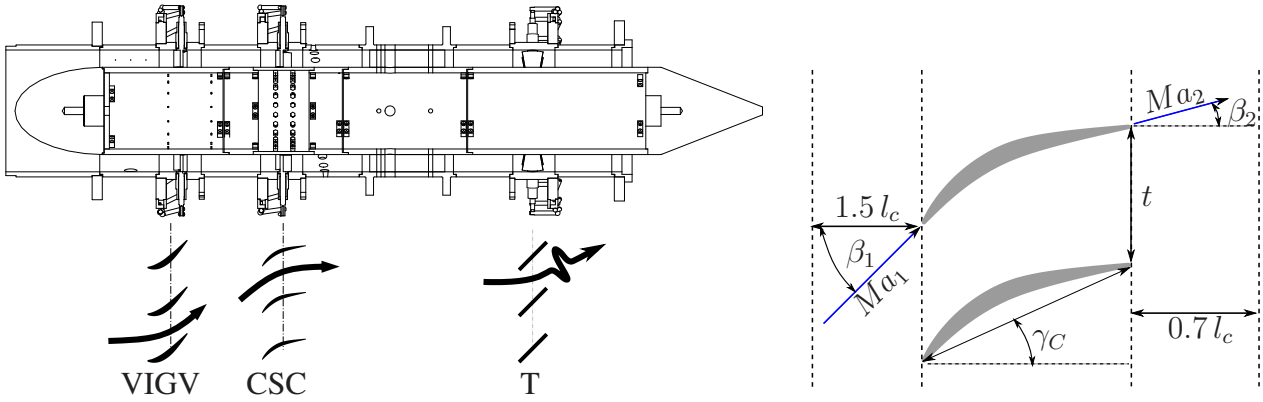

Figure 1: **Annular test rig and blade geometry.**

1 (right). The blades have an aspect ratio of 1, are similar to a controlled diffusion airfoil (CDA), and are very sensitive to flow separation. Thus, the hub clearance size is defined relative to the compressor blade chord length. Detailed data about the compressor stator cascade and the airfoils can be found in Beselt and Peitsch (2012) and Beselt et al. (2012).

To investigate the RI on the compressor stator cascade, different measurement techniques were used. The unsteady pressure distribution on the hub close to the LE and TE is measured by means of piezoresistive pressure transducers. The acoustic pressure waves emerging from the hub LE region are measured employing condenser microphones at the hub and the casing, upstream of the axial compressor cascade. The uncertainty of the unsteady pressure measurements is limited to $3\,\%$ of the measured pressure. A detailed description of the methods and their analysis can be found in Beselt and Peitsch (2012) and in Pardowitz et al. (2012b,a). Additionally, HS-PIV was used as an optical, non-intrusive measuring method, in order to obtain a complete picture of the RI phenomenon (see Sorge and Thamsen (2012)). The system was operated at a repetition rate of $5\,\mathrm{kHz}$ and recorded two velocity components of the flow field in a $1\,\mathrm{mm}$ thick plane. The plane was arranged tangential to the hub (see the small sketch in Figure 2). The mean particle shift was 5 to $8\,\mathrm{pixel}$ at a resolution of $16\,\mathrm{pixel/mm}$. Calibration and measurement uncertainties and perspective errors result in a total uncertainty of $2\,\%$ of the maximum for the determined velocities. During each HS-PIV measurement, a number of 8704 samples of the unsteady flow field were recorded, resulting in a measurement time period of $1.741\,\mathrm{s}$.

Numerical simulations

The numerical simulations are performed using the inhouse-code ELAN3D of the Department of Fluid Dynamics and Engineering Acoustics of the Berlin Institute of Technology, whose development has been initiated by Xue (1998). Pardowitz et al. (2012b) showed, that it is possible to assign azimuthal mode orders to each peak of the characteristic frequencies of the RI phenomenon. Thus, the full annulus of the compressor stator is simulated using the turbulence-resolving Delayed Detached-

Eddy Simulation (DDES) method proposed by Spalart et al. (2006), in order to capture all relevant azimuthal modes with the computational domain. The numerical mesh consist of 8.9 mio control volumes per passage. The axial extent of the computational domain is ≈ 2.5 chord lengths upstream and ≈ 3 chord lengths downstream of the blades leading and trailing edges, respectively. To ensure adequate temporal resolution, the unsteady flow field is calculated with a sample rate of $1\,\mathrm{MHz}$, which allows detailed analysis of unsteady flow features. Further details of the numerical mesh and additional information about the code and the setup for this configuration are given by van Rennings et al. (2012b). A number of $28\,000$ timesteps have been averaged to obtain the mean velocity field, in order to compare it with the time-averaged velocity field from the HS-PIV measurements.

RESULTS

Datum configuration

In previous studies, the dependence of the RI on the aerodynamic loading and the Mach number for a hub clearance of $3\,\%$ chord lengths were examined in detail. The result of these studies was that the best Signal to Noise Ratio (SNR) of the RI in the investigated compressor stator was determined at an incidence angle at midspan $i_M = 12°$, a Mach number of $\mathrm{Ma}_1 = 0.4$ and a Reynolds number of $\mathrm{Re} = 300\,000$ (see Beselt and Peitsch (2012) and Beselt et al. (2012)). For higher incidence angles, the magnitudes of the characteristic RI frequency patterns decreases for the chosen datum configuration.

In Figure 2, the time-averaged flow field in the LE region in a plane tangential to the hub acquired with the help of HS-PIV measurements is compared with the result from the numerical simulation for the datum configuration featuring RI. The comparison of the two time-averaged flow fields shows good agreement and allows the conclusion, that has been already drawn by Kameier and Neise (1997) and Beselt et al. (2012): A circumferentially spreading separation of the hub boundary layer is a necessary prerequisite for the occurrence of the RI. This behavior can be deduced from the time-averaged flow fields within the LE region, since the streamlines pass along the blades in circumferential direction. Along with this, the so-called *spilling forward* effect can be seen in the time-averaged flow fields, which is characterized by axial reverse flow across the LE from the pressure side to the suction side of one blade. For the case of the RI occurence and time averaged spilling forward, the three-dimensional coherent structures have been visualized using the λ_2 vortex criterion of Jeong and Hussain (1995). Three instantaneous snapshots from the numerical simulation are depicted in Figure 3 to illustrate the interaction of vortical structures with the blades LEs and the clearance flow within the passage entry region. It can be seen from the sequence of snapshots, that "tornado"-like vortices emerging from the hub boundary layer travel in circumferential direction with the mean flow and interact with the blade LEs. Subsequently, the clearance flow of the downstream passage in swirl direction is disturbed by the vortex that moves within the spilling forward flow across the blade LEs. Thereby, the clearance flow of the respective downstream passage collapses and originates new vortices, which in turn travel across with the meanflow to the adjacent downstream passage.

Figure 4 shows the averaged power spectral density function of axial and circumferential velocity fluctuations at three measurement points $5\,\mathrm{mm}$ upstream the LE and with $10\,\mathrm{mm}$ circumferential offset, respectively, obtained from HS-PIV measurements. The locations of the chosen positions are indicated in Figure 2. The instationary flow velocity time series taken exhibit the characteristic spectral pattern of the RI with frequency peaks of constant offset between 200 and $450\,\mathrm{Hz}$. Due to the short window length of $0.2\,\mathrm{s}$, the frequency resolution of the windowed spectral analysis was limited to $5\,\mathrm{Hz}$. However, the spectral pattern of the velocity fluctuations agrees well with the instationary pressure measurements of Pardowitz et al. (2012b) and Beselt and Peitsch (2012), respectively. For comparison, Figure 5 shows the results of the unsteady endwall pressure measurements using piezoresistive pressure transducers $1\,\mathrm{mm}$ upstream of the LE and $1\,\mathrm{mm}$ downstream of the TE. Upstream of

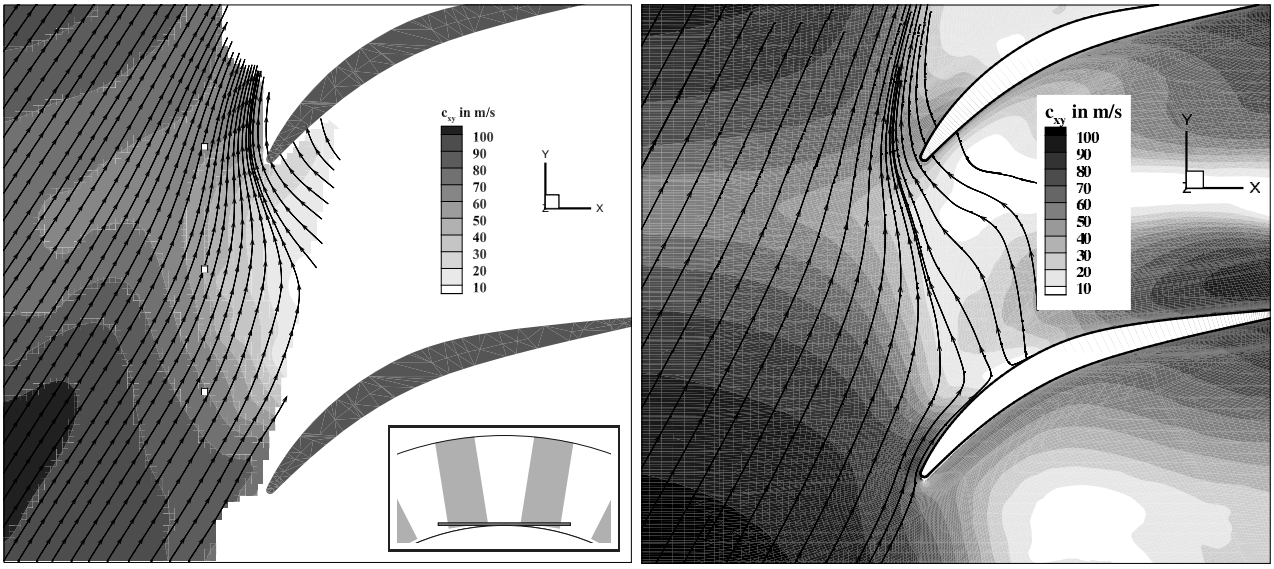

Figure 2: **Time averaged streamtraces and in-plane velocity magnitude distribution at** $\mathrm{Ma}_1 = 0.4$ **and** $i_M = 12°$ **in a plane tangential to the hub upstream of the compressor stator from the HS-PIV measurement (left) and the DDES computation (right). The measurement plane position is indicated in a small sketch in the left plot.**

Figure 3: **Visualization of coherent vortices in the instantaneous flow field in the LE region of the annular compressor blades derived from the numerical simulation. The coherent structures are visualized using an isosurface of the** λ_2**-criterion for the value** $-10^9\,1/\mathrm{s}^2$**.**

the LE, the characteristic properties of the RI can be seen in detail, whereas downstream of the TE no such patterns were recognized. In the case of stall or part-span stall in the compressor cascade, however, the mentioned characteristic properties should have been determined upstream **and** downstream of the blades.

In detail, a broad-band magnitude increase with side-by-side peaks and fixed frequency difference Δf of the frequency peaks in the PSD and coherence as well as a linear phase response in the frequency range of the side-by-side peaks were found. The linear phase response is an indicator for the circumferential propagation of the RI from the suction to the pressure side of the adjacent blade. The propagation velocity of the RI can be calculated using the linear phase response or the frequency difference between the side-by-side peaks. In both figures (4 and 5) as well in the velocity fluctuations as in the endwall pressure fluctuations the characteristic side-by-side peaks with constant frequency

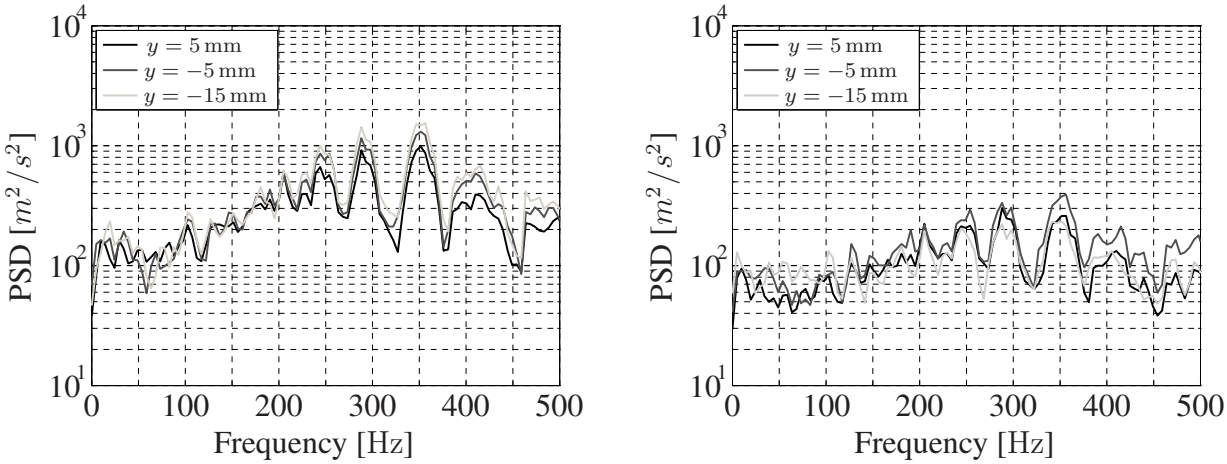

Figure 4: **Power spectral density function of axial (left) and circumferential (right) velocity fluctuations at reference conditions, analyzed $5\,\mathrm{mm}$ upstream of the compressor stator at three circumferentially distributed sensing points.**

differences Δf can be observed. The circumferential propagation speed of the RI yields from these values as well as from the gradient of the linear phase response to $35.3\,\mathrm{m/s}$. The resulting velocity corresponds to roughly $25\,\%$ of the circumferential main flow. According to Pardowitz et al. (2012a), the peak in the spectra at $130\,\mathrm{Hz}$ corresponds to an axial acoustic resonance of the test rig and can be disregarded in this context. In addition to the results of different types of pressure measurements,

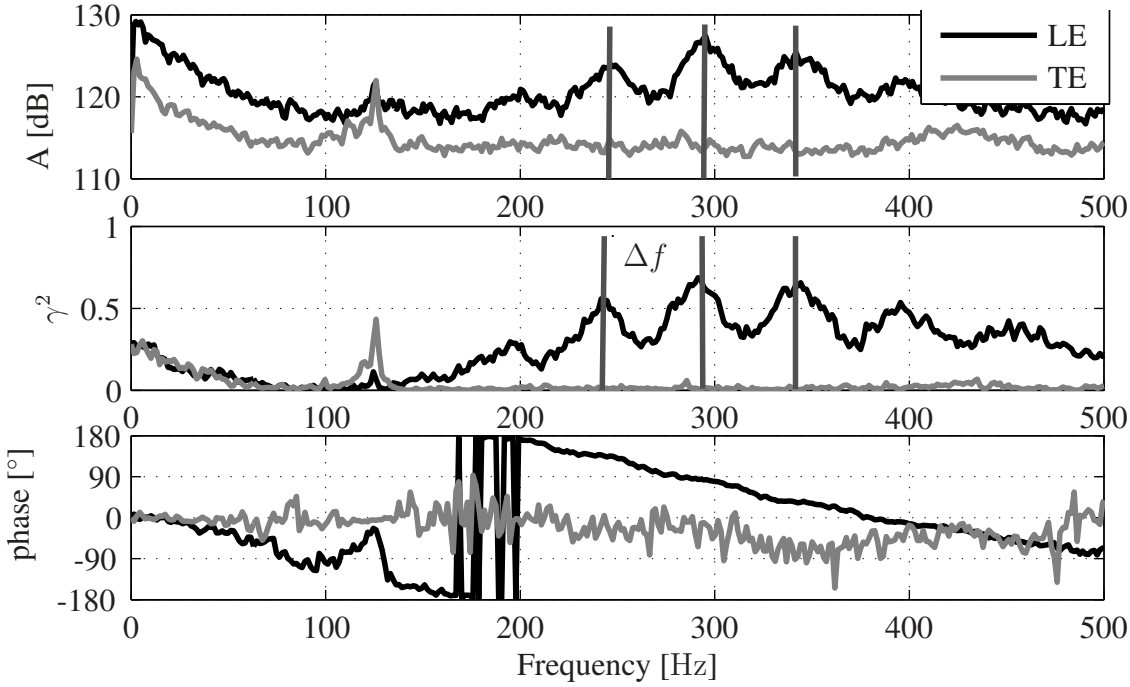

Figure 5: **Spectral analysis of the wall pressure fluctuations on the hub in the vicinity of the blades LE and TE at an incidence angle of $i_M = 11.3°$ for the datum configuration.**

the analysis of the HS-PIV data shows that the magnitudes of the frequencies of the axial velocity fluctuations are superior to the circumferential velocity fluctuations. This is in agreement with the assumption that an unsteady axial reverse flow at the blade LEs, on the pressure side, is necessary for RI.

Variation of clearance size

During the present study, a shift of the best SNR of the RI phenomenon to higher incidence angles with decreasing clearance sizes has been observed. For this reason, the clearance variation was carried out at a fixed incidence angle of $i_M = 16°$. At this operating point, the SNR of the RI for the hub clearances $\tau = 1\,\%\,l_c$ and $\tau = 0\,\%\,l_c$ is best and the SNR of the $\tau = 3\,\%\,l_c$ case still provides good results.

Figure 6 shows the cross-spectral density function (PSD), coherence, and phase angle of two $53°$ circumferentially displaced sensors $1\,\mathrm{mm}$ upstream of the compressor stator cascades leading edge at the hub for all investigated hub clearances. At all clearances, the characteristic features of the RI can be observed. These features are a broad-band magnitude increase exhibiting side-by-side frequency peaks with fixed frequency difference Δf in the PSD and coherence as well as a linear phase response in the frequency range of the side-by-side peaks. The highest magnitudes in the PSD are found at a hub clearance of $\tau = 1\,\%$ and the weakest at $\tau = 3\,\%$. The reason for this is the decreasing strength of the RI at higher incidence angles as shown in Beselt and Peitsch (2012). The gradient of the linear phase response for the $1\,\%$ and $0\,\%$ clearance size configuration differs from the reference configuration by about $5.7\,\%$ and $13.3\,\%$, respectively. The linear phase response is an indicator for the circumferential propagation of the RI from the suction side to the pressure side of the adjacent blade. The propagation velocity of the RI can be calculated using the linear phase response or the frequency difference between the side-by-side peaks. For the data shown in Figure 6, at all three investigated hub clearances of $3\,\%$, $1\,\%$, and $0\,\%$ the propagation velocity of the RI is $35.3\,\mathrm{m/s}$, $37.3\,\mathrm{m/s}$, and $40.0\,\mathrm{m/s}$, respectively. By comparing the results depicted in Figure 6 with the results of the HS-PIV measurements shown Figure 4 and the pressure measurements in Figure 5, a shift of the maximum magnitudes to lower frequencies is found. Furthermore, compared to Figure 5 an earlier inception of the linear phase response as well as a decreasing gradient of the linear phase response can be observed. This decrease corresponds to an increase in the propagation speed of the RI. A promotion of the RI due to an interaction of the clearance vortex flow with the mean flow is presumed, since the RI occurs typically in configurations with clearances at lower incidence angles and blade loadings. Simultaneously, the characteristic frequency of the RI increases compared to the configuration without clearance.

As shown in Figure 6, specific spectral signatures with side-by-side peaks are detected both for configurations with different clearance sizes as well as without a hub clearance. A more detailed analysis of these spectral signatures can be deduced from a circumferential mode analysis. Here, the modal patterns within the unsteady pressure field are determined upstream of the stator. The aim is to identify modal structures in accordance with typical RI patterns, which give strong evidence of the existence of the RI in all investigated cases.

A sensor ring equipped with 30 condenser microphones (type $^1/_4$" GRAS 40BP) is used to measure the unsteady pressure field $48\,\mathrm{mm}$ upstream of the stator leading edge wall-flush with the outer casing. Based on 30 sensors equidistantly spaced, an azimuthal mode analysis is feasible up to mode orders $m = \pm\,14$. This corresponds to a circumferential resolution of approximately 1.4 blade passages. The azimuthal mode decomposition used in this paper is described in detail in Pardowitz et al. (2012b). Here, cross spectra of all possible sensor combinations are determined leading to an improved statistical description of the unsteady pressure field. The analysis procedure in brief is as follows: The unsteady pressure field within a duct at fixed axial and radial positions can be described by a linear superposition of an infinite number of circumferential modes (cf. Mugridge (1969); Sijtsma and Zillmann (2007); Jürgens et al. (2010)). In matrix form as $p = Ga$, with the vector of circumferential mode amplitudes $a = (A_{-m}, \ldots, A_0, \ldots, A_m)$ and the matrix G of mode transfer functions, the cross spectral matrix of circumferential mode amplitudes A_{aa} can be calculated as a least-square estimate. The magnitude A_m of each mode of order m is deduced from the main diagonal in A_{aa}.

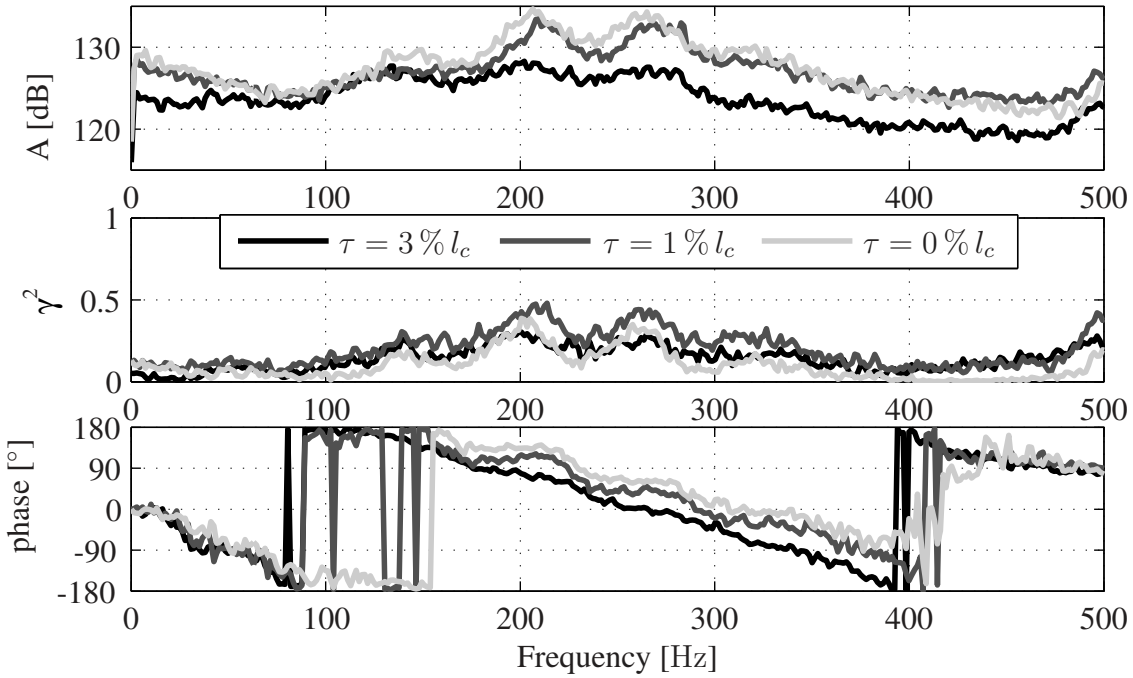

Figure 6: **Spectral analysis of the wall pressure fluctuations on the hub in the vicinity of the blades LE for three different hub clearances at an incidence angle of $i_M = 16°$.**

Similar to the results depicted in Figure 6, measurements were performed at three different hub clearance configurations at the chosen baseline operating condition (inflow Mach number of $\mathrm{Ma}_1 = 0.4$ and incidence of $i_M = 16°$). In each case, the mode amplitudes are calculated over a wide frequency range. Magnitudes of selected modes of orders up to $m = +7$ are depicted in Figure 7 for frequencies up to $500\,\mathrm{Hz}$. Side-by-side peaks with significant magnitudes are visible with subsequently numbered circumferential mode orders from $m = +1$ up to $+5$. The maxima of the mode magnitudes are in correspondence with the peaks of the averaged spectra measured next to the leading edge (compare Figure 6 and Figure 7). These patterns are typically attributed to the RI phenomenon. Differences between the measured spectral magnitudes and the determined mode amplitudes in the upstream field are explained by an exponential decay of non propagating modes in the duct. Amplitudes of higher mode orders exhibit a higher decay rate. As a consequence, the characteristic modal signature (with its relative amplitudes) is changed with respect to its distance from the physical source plane. This behaviour is observed by comparing the spectra in the nearfield (Figure 6) with the modal patterns acquired with the upstream microphone array (Figure 7).

The detected modal patterns reveal that the RI phenomenon consists of characteristic spectral components spread over a wide frequency range. In contrast, at a single sensor only the dominant peaks of the RI signature are clearly visible. Consequently, the characteristic frequency spacings $\Delta f_{m;m+1}$ between adjacent RI modes m and $m+1$ can be determined more precisely with the help of the applied analysis technique. It is recognized that the characteristic frequency spacings are not constant within the RI-pattern. This is contrary to the common characterisation of the RI phenomenon, where a constant frequency spacing suggests a uniform rotation of the phenomenon. A possible explanation for this finding is a circumferential wave dispersion effect, resulting in different circumferential propagation velocities for different modes, respectively. Another noteworthy modal property was identified in earlier studies Pardowitz et al. (2012b). It was pointed out that each RI mode in the modal pattern occurs stochastically distributed in time. Moreover, modes of different circumferential orders were found to be incoherent, i.e. stochastically independent from each other.

In summary, the applied mode analysis method enables an identification of the RI, although the microphone array is placed in the outer casing upstream of the stator. A comparison of the three hub clearance configurations at similar operating conditions yields that the modal RI pattern exists in each case, albeit exhibiting small changes of amplitudes and frequencies. This finding is in contradiction to common explanations of the RI phenomenon, where the unsteady clearance vortex is assumed to be the initiating mechanism of the RI (cf. e.g. Schrapp et al. (2009) and Mailach et al. (2001)). The theory modelling the RI phenomenon as a rotating noise source (mainly coined by Kameier (1994) and Kameier and Neise (1997)) is not in line with the stochastic independence of different RI modes. Further, the theoretical model assumes a constant frequency spacing between side-by-side peaks, which could not be confirmed (see Figure 7) in this study. Thus, a new explanation about the RI phenomenon is needed.

A new hypothesis of the basic RI mechanism was developed in Pardowitz et al. (2012b), implying that shear layer instability waves of different wavelengths are generated at stochastically distributed moments in time and subsequently propagate in circumferential direction. At highly loaded operating conditions and large clearance sizes, a significant leakage flow exist. Thus, at the leading edge, a radial flow profile of the axial velocity develops which exhibits regions of reversed flow (here simply interpreted as prove for a shear layer). Generally, shear layers are prone for flow instabilities (Drazin and Reid (1981) and Huerre and Monkewitz (1985)). Instability waves are generated with different wavelengths, various growth rates and propagation velocities. At flow conditions, where the region of reversed flow arises over the whole cirumference, instability waves can propagate in the circumferential direction. It is assumed, that at certain frequencies and wavelengths, a resonant condition over the whole circumference is met, respectively seen as one of the typical RI modes.

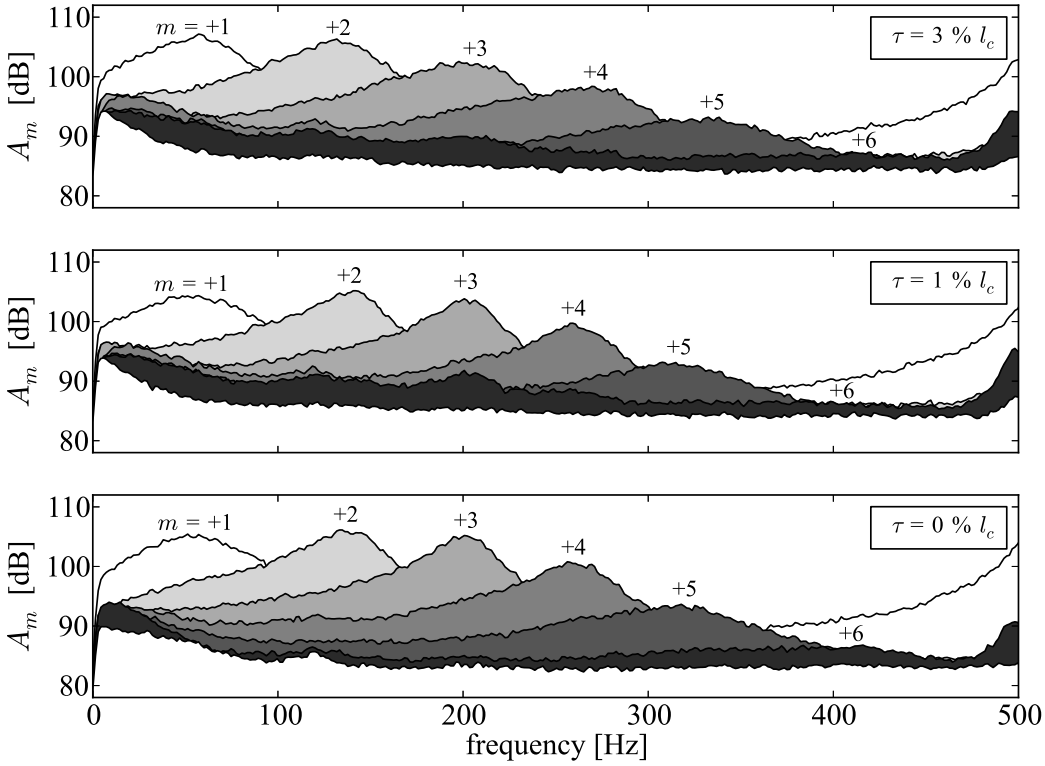

Figure 7: **Azimuthal mode magnitudes in the upstream section of the stator** $-48\,\mathrm{mm}$ **distance to the leading edge comparing the three hub clearance configurations at similar operating conditions (**$\mathrm{M}_1 = 0.4$ **and incidence** $i_M = +16°$**).**

CONCLUSIONS

This paper presents an extensive study about the rotating instability phenomenon on an annular compressor cascade. Unsteady aerodynamic and acoustic pressure measurements, high-speed Particle Image Velocimetry measurements, and turbulence resolving numerical simulations were conducted. The objective was to improve the understanding of the RI source mechanism. A variation of the hub clearance of the stator blades revealed the surprising occurrence of the rotating instability down to low clearances and even in a configuration without hub clearance. Typical spectral RI signatures were identified next to the stator blade leading edges by means of the unsteady flow field acquired via high speed PIV as well as unsteady pressure measurements. Characteristic RI frequencies and amplitude shapes were detected. For each examined case, a circumferential mode analysis technique delivered distinct modal patterns of the RI. These results are in accordance with former findings in the literature, eg. Kameier and Neise (1997); Mailach et al. (2001); Schrapp et al. (2009) . However, the experimental results for the absence of a hub clearance are in contradiction to existing theoretical RI models from literature. As a reason of that, an alternative formulation of the source mechanism of the RI phenomenon has to be found. A new hypothesis about the RI source mechanism was developed by Pardowitz et al. (2012b), implying that shear layer instability waves of different wavelengths are generated at stochastically distributed moments in time and subsequently propagate in circumferential direction. Further, it is assumed that interactions between secondary flow structures in the end wall region of the blade passages, e.g. the horseshoe or corner vortex, initiate the RI phenomenon. The authors believe that the originated vortices travel subsequently in circumferential direction and interact with the other blade leading edges. This process is likely to be the aerodynamic source mechanism of the characteristic spectral patterns related to the RI. More detailed investigations without hub clearance are planned in the near future. They will further enhance the knowledge about the RI phenomenon and its associated unsteady vortex structures in the blade passages of axial turbomachines.

ACKNOWLEDGEMENTS

The presented work has been carried out within the framework of the research projekt “Flow induced Acoustics in Turbomachines – The Rotating Instability” funded by the German Research Foundation (DFG). The results of the numerical computations have been produced on the Supercomputer HLRN-II of the North-German Supercomputing Alliance (HLRN) at the Konrad-Zuse-Zentrum für Informationstechnik Berlin (ZIB). The authors would like to thank both institutions for kindly supporting this investigation.

REFERENCES

Baumgartner, M., Kameier, F., and Hourmouziadis, J. (1995). Non-engine order blade vibration in a high pressure compressor. In *ISABE - Twelfth International Symposium on Airbreathing Engines, Melbourne, Australia, 10-15 September*.

Beselt, C. and Peitsch, D. (2012). Influence of mach number and aerodynamic loading on rotating instability in an annular compressor cascade. In *Proceedings of ASME Turbo Expo 2012, June 11–15, 2012, Copenhagen, Denmark*.

Beselt, C., Peitsch, D., Pardowitz, B., and Enghardt, L. (2011). Strömungsinduzierter Schall in Turbomaschinen – Die Rotierende Instabilität. In *DGLR Jahrestagung, 27.–29. September 2011, Bremen*.

Beselt, C., van Rennings, R., Thiele, F., and Peitsch, D. (2012). Experimental and numerical investigation of rotating instability phenomenon in an axial compressor stator. In *Proceedings of 42nd AIAA Fluid Dynamics Conference and Exhibit, 25.–28. June 2012, Sheraton, New Orleans*.

Cumpsty, N. (2004). *Compressor Aerodynamics*. Krieger Publishing Company.

Drazin, P. G. and Reid, W. H. (1981). *Hydrodynamic stability*. Cambridge University Press.

Hofmann, W., Kameier, F., Schnittfeld, T., Thiele, F., and Wenger, U. (1998). Analyse transienter Meßdaten eines zehnstufigen Hochdruckverdichters an der Stabilitätsgrenze. *VDI Berichte*, 1425:211–223.

Huerre, P. and Monkewitz, P. A. (1985). Absolute and convective instabilities in free shear layers. *Journal of Fluid Mechanics*, 159:151–168.

Inoue, M., Kuroumaru, M., Yoshida, S., Minami, T., Yamada, K., and Furukawa, M. (2004). Effect of tip clearance on stall evolution process in a low-speed axial compressor stage. *ASME Conference Proceedings*, 2004(41707):385–394.

Jeong, J. and Hussain, F. (1995). On the identification of a vortex. *Journal of Fluid Mechanics*, 285:69–94.

Jürgens, W., Tapken, U., Pardowitz, B., Kausche, P., Bennett, G., and Enghardt, L. (2010). Technique to analyze characteristics of turbomachinery broadband noise sources. In *16th AIAA/CEAS Aeroacoustics Conference*.

Kameier, F. (1994). *Experimentelle Untersuchung zur Entstehung und Minderung des Blattspitzen-Wirbellärms axialer Strömungsmaschinen*. PhD thesis, Technische Universität Berlin / Deutsches Zentrum für Luft- und Raumfahrt (DLR).

Kameier, F. and Neise, W. (1997). Rotating blade flow instability as a source of noise in axial turbomachines. *Journal of Sound and Vibration*, 203(5):833–853.

Mailach, R., Lehmann, I., and Vogeler, K. (2001). Rotating instabilities in an axial compressor originating from the fluctuating blade tip vortex. *Journal of Turbomachinery*, 123(3):453–460.

Mugridge, B. (1969). The measurement of spinning acoustic modes generated in an axial flow fan. *Journal of Sound and Vibration*, 10(2):227 – 246.

März, J., Hah, C., and Neise, W. (2002). An experimental and numerical investigation into the mechanisms of rotating instability. *Journal of Turbomachinery*, 124(3):367–374.

Pardowitz, B., Tapken, U., and Enghardt, L. (2012a). Acoustic resonances and aerodynamic interactions in an axial compressor stator stage test rig. In *10th International Conference on Flow-Induced Vibration (& Flow-Induced Noise), 2nd – 6th July 2012, Dublin*.

Pardowitz, B., Tapken, U., and Enghardt, L. (2012b). Time-resolved rotating instability waves in an annular cascade. In *18th AIAA/CEAS Aeroacoustics Conference, 4. – 6. June 2012, Colorado Springs, Colorado*.

Schrapp, H. (2008). *Experimentelle Untersuchungen zum Aufplatzen des Spaltwirbels in Axialverdichtern*. PhD thesis, Technische Universität Braunschweig.

Schrapp, H., Stark, U., and Satthoff, H. (2009). Unsteady behaviour of the tip clearance vortex in a rotor equivalent compressor cascade. *Journal of Power and Engineering*, 223:635–643.

Sijtsma, P. and Zillmann, J. (2007). In-duct and far-field mode detection techniques for engine exhaust noise measurements. In *13th AIAA/CEAS Aeroacoustics Conference*, number 2007-3439.

Sorge, R. and Thamsen, P. U. (2012). Experimental investigations of rotating instabilities in a steady turbine grid with high speed particle image velocimetry. In *Conference on Modelling Fluid Flow, 4. – 7. September 2012, Budapest, Hungary*.

Spalart, P., Deck, S., Shur, M., Squires, K., Strelets, M., and Travin, A. (2006). A new version of detached-eddy simulation, resistant to ambiguous grid densities. *Theoretical and Computational Fluid Dynamics*, 20:181–195.

van Rennings, R., Ehrenfried, K., and Thiele, F. (2012a). Modelling of the dynamics and acoustic emissions of rotating instability in an annular compressor cascade. In *Proceedings of the 9th European Conference on Noise Control, 10.–13. June 2012, Prague, Czech Republic*. ISBN 978-80-01-05013-2, ISSN 2226-5147.

van Rennings, R., Shi, K., Fu, S., and Thiele, F. (2012b). Delayed-detached-eddy simulation of near-stall axial compressor flow with varying passage numbers. In Fu, S., Haase, W., Peng, S.-H., and Schwamborn, D., editors, *Progress in Hybrid RANS-LES Modelling*, volume 117 of *Notes on Numerical Fluid Mechanics and Multidisciplinary Design*, pages 439–448. Springer Berlin / Heidelberg.

Weidenfeller, J. and Lawerenz, M. (2002). Time resolved measurements in an annular compressor cascade with high aerodynamic loading. *ASME Conference Proceedings*, 2002(3610X):751–758.

Xue, L. (1998). *Entwicklung eines effizienten parallelen Lösungsalgorithmus zur dreidimensionalen Simulation komplexer turbulenter Strömungen*. PhD thesis, Technische Universität Berlin.